29th International Congress on Sound and Vibration
The annual congress of the International Institute of Acoustics and Vibration (IIAV)
9–13 July 2023
ICSV29

# A RAILWAY VEHICLE-ELECTROMAGNETIC SUSPENSION COUPLING SYSTEM FOR VIBRATION REDUCTION WITH ENERGY HARVESTING

Jing Tang Xing
*Maritime Engineering, CMEE, FEPS, University of Southampton, Southampton, UK*
*email: jtxing@soton.ac.uk*

Li Qin
*Key Laboratory of Metallurgical Equipment & Control Technology, SMA, WUST, Wuhan, PRC*
*e-mail: Qinli429@wust.edu.cn*

This paper investigates a railway vehicle-electromagnetic energy harvester coupling system subject to external excitations to provide a modelling for designing effective suspensions to harvest energies and reduce vibrations. Following the proposed generalised mathematical model with solution method, a beam-like vehicle system is solved. The results of track and aerodynamic excitations show that with increasing energy harvesting parameter, vibrations are reduced while the harvested power increased, so that a comfortable ride performance is reached. The paper provides a means to design effective suspension units for high-speed trains to reduce vibrations and harvester energies.

Keywords: Vibration energy harvesters, Electromagnetic-suspensions, Vibration reductions, Mechanical electromagnetic interactions, Railway vehicle dynamics.

## 1. Introduction

Environmental concerns and energy price increases have accelerated the global trend toward two research directions. One is seeking green energies harvested by energy converters [1-4]. Papers [3,4] provide details of various energy harvesters with references. Another is to develop designs to reduce energy waste by harvesting vibration energies in transports. There have been papers dealing with different designs to harvest vibration energy [5,6]. Regenerative suspensions in harvesting energies while reducing vibrations are reported, of which details can be referred in the review papers [7~10]. Electromagnetic energy harvester is an electric system, which is connected into a vehicle results a mechanical – electrical coupling system. For effective designs, an interdisciplinary study is necessary. Paper [11] investigated this type of system to reveal its coupling effects. This paper investigates a railway vehicle-electromagnetic coupling system to provide a modelling for effective vibration reductions and energy harvesting in high-speed trains.

## 2. Mathematical Modelling

Figure 1 (a) shows a railway vehicle as an elastic body $\Omega$ of length $L$, width $b$, height $H$ and mass density $\rho$, subject to an aerodynamic force $f(\boldsymbol{X}, t)$. At mass center $O$, a vehicle system $O-XYZ$ is fixed. The system $o-xyz$ is fixed at point $o$ in space, where the train moves in velocity $V$ in $y$ direction. The

vehicle is supported by 4 electromagnetic suspension units (Fig. 1b) at points $\boldsymbol{X}_I(X_I, Y_I, Z_I)$, ($I$ = 1,2,3,4). We assume that the front and tail bogies are two rigid bodes only allowing vertical motion, so that there is two degrees of freedom for each bogie, modelled by two rigid masses $m_I^b$ of displacement $Z_I$, connected to the wheel through spring $k_I$ and damper $c_I$. The wheel is considered as a rigid mass subject to track excitation $h(x_I, t)$. To reduce vibrations, there are 4 suspension units to support the vehicle, each consisting of spring $K_I$ and damper $C_I$, connected to a magnetic body of mass $m_I$ fixed on the bogie. An electric coil of mass $m_I^c$ is rigid connected to vehicle at point $\boldsymbol{X}_I$, moving with the vehicle cross the magnetic field, so that an induced voltage produced on the two coil terminals connected to an energy collector $R_I$. Therefore, there is an electric current flowing in the coil producing an electromagnetic force against vehicle motion to reduce vibrations and harvest energy.

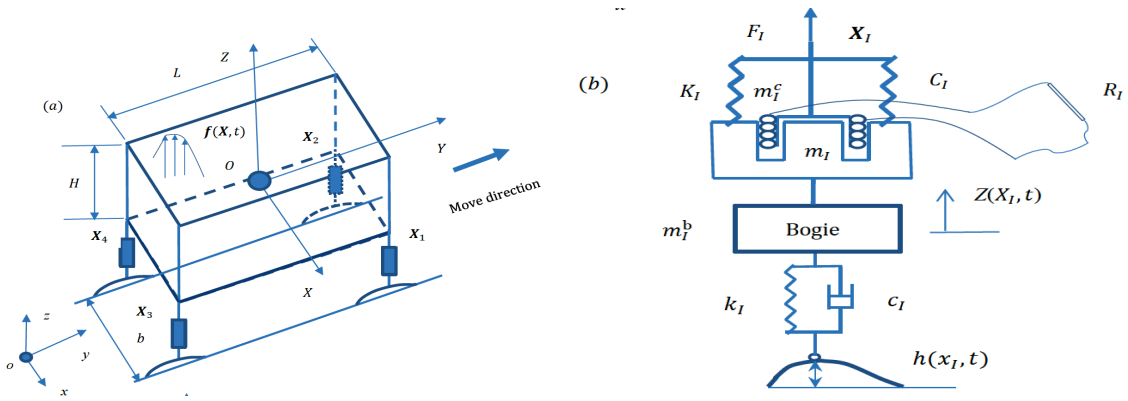


Figure 1: A railway vehicle-energy harvester interaction system with 4 electromagnetic suspension units fixed at points $X_I$, : (a) integrated arrangement; (b) details of a suspension unit at $X_I$.

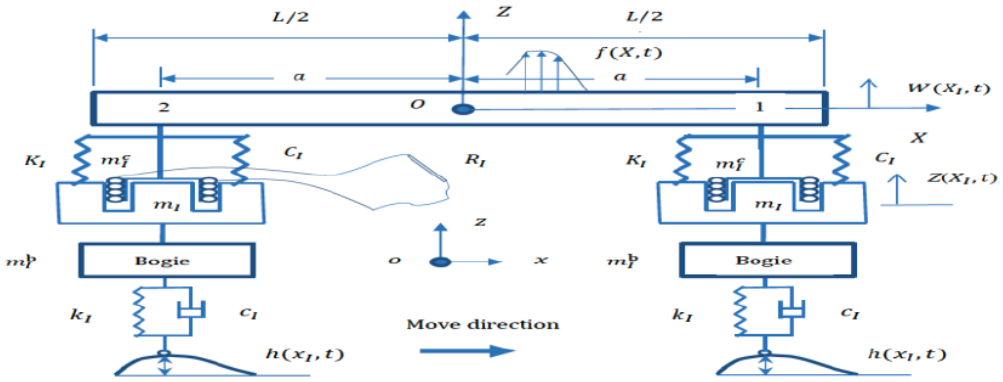


Figure 2: A half-integrated railway beam-like vehicle-energy harvester interaction system.

## 2.1 Dynamic Equation of Elastic Vehicle

Vertical displacement $U(X_i, t)$, ($i$ = 1,2,3) as tensor index, of a free-free vehicle satisfies

$$E_{3j3l}U_{,lj} - \sum_{I=1}^{4} F_I\,\Delta(\boldsymbol{X}-\boldsymbol{X}_I) + f(\boldsymbol{X},t)\Delta(\widetilde{\boldsymbol{X}}-\boldsymbol{X}) = \rho\frac{\mathrm{d}^2U}{\mathrm{d}t^2},\ \ \boldsymbol{X}\in\Omega;\ E_{3j3l}U_{,l}\nu_j = 0,\ \ \boldsymbol{X}\in S, \qquad (2\text{-}1)$$

where $()_{k,l} = \partial()_k/\partial X_l$, $F_I$ is a supporting force at $\boldsymbol{X}_I$, and $E_{ijkl}$ is elastic tensor, $\Delta()$ is a Delta function.

## 2.2 Motion of Bogie and Magnetic Body

Force $F_I$ in Eq. (2-1) is a suspension force at point $\boldsymbol{X}_I$, of which the positive value is defined as a pulling force of body,

$$F_I = K_I[U_{3I} - Z_I] + C_I\left[\dot{U}_{3I} - \dot{Z}_I\right] + \hat{F}_I + m_I^c\ddot{U}_{3I}, \tag{2-2}$$

$$\left(m_I + m_I^{\mathrm{b}}\right)\ddot{Z}_I + (C_I + c_I)\dot{Z}_I + (k_I + K_I)Z_I - K_I\boldsymbol{U}_{3I} - C_I\dot{U}_{3I} - \hat{F}_I = k_I h(x_I, t) + c_I\dot{h}(x_I, t).$$

## 2.3 Energy Harvesting Converter

The energy harvesting converter $I$ consists of a magnetic body of intensity $B_I$ and an electric coil with its effective length $l_I$, electrical inductance $L_I$, resistance $r_I$ and capacitance $\widehat{C}_I$. The coil moves cross the electromagnetic field producing the induced voltage $e_I$ at the two ends of power resistance $R_I$, so that an electric charge $Q_I$ with current $I_I$ is generated in the moving coil, from which an electromagnetic force $\hat{F}_I$ against the motion is produced. Laplace theorem and electrical equilibrium principle give

$$e_I = B_I l_I\left(\dot{U}_3(\boldsymbol{X}_I, t) - \dot{Z}_I\right), \quad \hat{F}_I = I_I B_I l_I = \dot{Q}_I B_I l_I, \quad U_I = U_3(\boldsymbol{X}_I, t), \tag{2-3}$$

$$e_I = L_I\ddot{Q}_I + (R_I + r_I)\dot{Q}_I + Q_I/\hat{C}_I = L_I\dot{I}_I + (R_I + r_I)I_I + \int I_I\mathrm{d}t/\hat{C}_I, \quad I_I = \dot{Q}_I, \tag{2-4}$$

$$L_I\ddot{Q}_I + (R_I + r_I)\dot{Q}_I + Q_I/\hat{C}_I - B_I l_I\left(\dot{U}_I - \dot{Z}_I\right) = 0, \tag{2-5}$$

which is coupled with Eq. (2-1). Considering that the capacitance $\widehat{C}_I$ of coil is quite large, and the inductance $L_I$ is small, we approximate Eqs. (2-3~4) into

$$(R_I + r_I)\dot{Q}_I = (R_I + r_I)I_I = B_I l_I\left(\dot{U}_I - \dot{Z}_I\right), \tag{2-6}$$

from which, when using Eq. (2-3), it follows the electromagnetic force

$$\hat{F}_I = \frac{(B_I l_I)^2}{R_I + r_I}\left(\dot{U}_I - \dot{Z}_I\right) = C_I^e\left(\dot{U}_I - \dot{Z}_I\right), \quad C_I^e = \frac{(B_I l_I)^2}{R_I + r_I}. \tag{2-7}$$

Here, $C_I^e$ is the *energy harvesting coefficient of energy converter*. The collected power of converter $I$ is

$$\hat{P}_I = I_I^2 R_I = \frac{C_I^e R_I}{R_I + r_I}\left(\dot{U}_I - \dot{Z}_I\right)^2 = \frac{C_I^e R_I}{R_I + r_I}[\dot{U}_I \quad \dot{Z}_I]\begin{bmatrix}1 & -1\\ -1 & 1\end{bmatrix}\begin{bmatrix}\dot{U}_I\\ \dot{Z}_I\end{bmatrix}, \quad \hat{P} = \sum_{I=1}^4 \hat{P}_I, \tag{2-8}$$

of which the percentages of energy collection and its time average are given by

$$\lambda_I = \hat{P}_I/P_I, \quad \bar{\lambda}_I = \langle\hat{P}_I\rangle/\langle P_I\rangle, \quad \lambda = \hat{P}/P, \quad \bar{\lambda} = \langle\hat{P}\rangle/\langle P\rangle. \tag{2-9}$$

## 2.4 Mechanical-Electric Coupled Equation

### *2.4.1 Mode equation of railway vehicle body*

Modes and frequencies of vehicle obtained by finite element analysis are used in a mode summation approach to express displacement $U_3(\boldsymbol{X}, t) = U(\boldsymbol{X}, t)$ in the matrix form

$$U(\boldsymbol{X}, t) = \boldsymbol{\Phi}\boldsymbol{q}, \qquad \boldsymbol{\Phi} = [\phi_1 \quad \phi_2 \quad \cdots \quad \phi_N], \quad \boldsymbol{q} = [q_1 \quad q_2 \quad \cdots \quad q_N]^{\mathrm{T}}, \tag{2-10}$$

where $\boldsymbol{\Phi}$ is a mode matrix of $\phi_n$, and $\boldsymbol{q}$ generalised coordinate, and $N$ is retained mode number. Substituting Eq. (2-10) into Eq. (2-1), pre-multiplying both sides by $\boldsymbol{\Phi}^{\mathrm{T}}$ we obtain

$$(\boldsymbol{M} + \boldsymbol{m}^c)\ddot{\boldsymbol{q}} + \boldsymbol{C}\dot{\boldsymbol{q}} + (\boldsymbol{\Lambda} + \boldsymbol{K})\boldsymbol{q} - \boldsymbol{K}_1^z Z_1 - \boldsymbol{K}_2^z Z_2 - \boldsymbol{C}_1^z\dot{Z}_1 - \boldsymbol{C}_2^z\dot{Z}_2 + \boldsymbol{B}_1\dot{Q}_1 + \boldsymbol{B}_2\dot{Q}_2 = \boldsymbol{F}, \tag{2-11,12,13}$$

$$\boldsymbol{M} = \boldsymbol{I}_{N\times N} = \int_\Omega \boldsymbol{\Phi}^T\rho\boldsymbol{\Phi}\mathrm{d}\Omega, \quad \boldsymbol{\Lambda} = \int_\Omega \boldsymbol{\Phi}_{,j}^T E_{3j3l}\boldsymbol{\Phi}_{,l}\mathrm{d}\Omega, \quad \boldsymbol{F} = \int_\Omega \boldsymbol{\Phi}^{\mathrm{T}} f(\boldsymbol{X}, t)\mathrm{d}\Omega, \boldsymbol{K}_I^z = \boldsymbol{\Phi}^T(\boldsymbol{X}_I)K_I,$$

$$\boldsymbol{C}_I^z = \boldsymbol{\Phi}^T(\boldsymbol{X}_I)C_I, \quad \boldsymbol{m}^c = \sum_{I=1}^4\{\boldsymbol{\Phi}^T(\boldsymbol{X}_I)m_I^c\boldsymbol{\Phi}(\boldsymbol{X}_I)\}, \quad \boldsymbol{K} = \sum_{I=1}^4\{\boldsymbol{\Phi}^T(\boldsymbol{X}_I)K_I\boldsymbol{\Phi}(\boldsymbol{X}_I)\},$$

$$\boldsymbol{C} = \sum_{I=1}^4\{\boldsymbol{\Phi}^T(\boldsymbol{X}_I)C_I\boldsymbol{\Phi}(\boldsymbol{X}_I)\}, \quad \boldsymbol{B}_I = \boldsymbol{\Phi}^T(\boldsymbol{X}_I)B_I l_I, \quad \boldsymbol{\Lambda} = \mathrm{diag}\left(\omega_J^2\right), \quad J = 1,2,\cdots,N.$$

The first three frequencies $\omega_{1,2,3} = 0$ are three rigid modes

Pitching: $\phi_1(\boldsymbol{X}) = 2\sqrt{3}Y/\left(\sqrt{J_1}L\right)$, Rolling: $\phi_2(\boldsymbol{X}) = 2\sqrt{3}X/\left(\sqrt{J_2}b\right)$, Heave: $\phi_3(\boldsymbol{X}) = 1/\sqrt{M}$, (2-14)

where the vehicle as a center-symmetrical structure of total mass $M$ has its pitching and rolling inertia $J_1$and $J_2$. Similarly, we obtain the equations of bogie and electric circuit

$$\left(m_I + m_I^{\mathrm{b}}\right)\ddot{Z}_I + (K_I + k_I)Z_I + (C_I + c_I)\dot{Z}_I - \boldsymbol{K}_I^{zT}\boldsymbol{q} - \boldsymbol{C}_I^{zT}\dot{\boldsymbol{q}} - \dot{Q}_I B_I l_I = k_I h(x_I, t) + c_I \dot{h}(x_I, t), \quad (2\text{-}15)$$

$$L_I\ddot{Q}_I + (R_I + r_I)\dot{Q}_I + Q_I/\hat{C}_I - B_I l_I \boldsymbol{\Phi}(\boldsymbol{X}_I)\dot{\boldsymbol{q}} + B_I l_I \dot{Z}_I = 0. \quad (2\text{-}16)$$

### 2.4.2 Matrix form of coupled equation

Equations (2-11~16) can be re-written in a matrix form

$$\begin{bmatrix} \boldsymbol{M} + \boldsymbol{m}^c & \boldsymbol{0} & \boldsymbol{0} \\ \boldsymbol{0} & \boldsymbol{m} & \boldsymbol{0} \\ \boldsymbol{0} & \boldsymbol{0} & \boldsymbol{L} \end{bmatrix}\begin{bmatrix} \ddot{\boldsymbol{q}} \\ \ddot{\boldsymbol{Z}} \\ \ddot{\boldsymbol{Q}} \end{bmatrix} + \begin{bmatrix} \boldsymbol{C} & -\boldsymbol{C}^z & \boldsymbol{B}^T \\ -\boldsymbol{C}^{zT} & \boldsymbol{c} & -\boldsymbol{B}^z \\ -\boldsymbol{B} & \boldsymbol{B}^z & \boldsymbol{R} \end{bmatrix}\begin{bmatrix} \dot{\boldsymbol{q}} \\ \dot{\boldsymbol{Z}} \\ \dot{\boldsymbol{Q}} \end{bmatrix} + \begin{bmatrix} \boldsymbol{\Lambda} + \boldsymbol{K} & -\boldsymbol{K}^z & \boldsymbol{0} \\ -\boldsymbol{K}^{zT} & \boldsymbol{k} & \boldsymbol{0} \\ \boldsymbol{0} & \boldsymbol{0} & \widehat{\boldsymbol{C}} \end{bmatrix}\begin{bmatrix} \boldsymbol{q} \\ \boldsymbol{Z} \\ \boldsymbol{Q} \end{bmatrix} = \begin{bmatrix} \boldsymbol{F} \\ \boldsymbol{f} \\ \boldsymbol{0} \end{bmatrix}, \quad (2\text{-}17)$$

$$\boldsymbol{Z}^T = [Z_1 \quad Z_2 \quad Z_3 \quad Z_4], \quad \boldsymbol{K}^z = [\boldsymbol{K}_1^z \quad \boldsymbol{K}_2^z \quad \boldsymbol{K}_3^z \quad \boldsymbol{K}_4^z], \quad \boldsymbol{C}^z = [\boldsymbol{C}_1^z \quad \boldsymbol{C}_2^z \quad \boldsymbol{C}_3^z \quad \boldsymbol{C}_4^z],$$

$$\boldsymbol{Q}^T = [Q_1 \quad Q_2 \quad Q_3 \quad Q_4], \quad \boldsymbol{f}^T = [f_1 \quad f_2 \quad f_3 \quad f_4], \quad f_I = k_I h(x_I, t) + c_I \dot{h}(x_I, t), \quad (2\text{-}18)$$

$$\boldsymbol{m} = \mathrm{diag}\left(m_I + m_I^{\mathrm{b}}\right), \ \boldsymbol{c} = \mathrm{diag}(C_I + c_I), \quad \boldsymbol{k} = \mathrm{diag}(K_I + k_I), \ \boldsymbol{B} = [\boldsymbol{B}_1 \quad \boldsymbol{B}_2 \quad \boldsymbol{B}_3 \quad \boldsymbol{B}_4]^T,$$

$$\boldsymbol{B}^z = \mathrm{diag}(B_I l_I), \quad \boldsymbol{L} = \mathrm{diag}(L_I), \quad \boldsymbol{R} = \mathrm{diag}(R_I + r_I), \quad \widehat{\boldsymbol{C}} = \mathrm{diag}\left(1/\hat{C}_I\right). \ I = 1,2,3,4,$$

of which the damping matrix is non-symmetrical. By considering that the capacitance $\widehat{C_I}$ of coil is quite large, and inductance $L_I$ is very small, electric equation in Eq. (2-17) vanishes and current $\boldsymbol{I}$ is given

$$\boldsymbol{R}\dot{\boldsymbol{Q}} - \boldsymbol{B}\dot{\boldsymbol{q}} + \boldsymbol{B}^z\dot{\boldsymbol{Z}} = \boldsymbol{0}, \qquad \boldsymbol{I} = \dot{\boldsymbol{Q}} = \boldsymbol{R}^{-1}\boldsymbol{B}\dot{\boldsymbol{q}} - \boldsymbol{R}^{-1}\boldsymbol{B}^z\dot{\boldsymbol{Z}}, \quad (2\text{-}19,20)$$

which, when substituted into Eq. (2-17), gives

$$\begin{bmatrix} \boldsymbol{M} + \boldsymbol{m}^c & \boldsymbol{0} \\ \boldsymbol{0} & \boldsymbol{m} \end{bmatrix}\begin{bmatrix} \ddot{\boldsymbol{q}} \\ \ddot{\boldsymbol{Z}} \end{bmatrix} + \{\boldsymbol{C}^m + \boldsymbol{C}^e\}\begin{bmatrix} \dot{\boldsymbol{q}} \\ \dot{\boldsymbol{Z}} \end{bmatrix} + \begin{bmatrix} \boldsymbol{\Lambda} + \boldsymbol{K} & -\boldsymbol{K}^z \\ -\boldsymbol{K}^{zT} & \boldsymbol{k} \end{bmatrix}\begin{bmatrix} \boldsymbol{q} \\ \boldsymbol{Z} \end{bmatrix} = \begin{bmatrix} \boldsymbol{F} \\ \boldsymbol{f} \end{bmatrix}, \quad (2\text{-}21)$$

$$\boldsymbol{C}^m = \begin{bmatrix} \boldsymbol{C} & -\boldsymbol{C}^z \\ -\boldsymbol{C}^{zT} & \boldsymbol{c} \end{bmatrix}, \quad \boldsymbol{C}^e = \begin{bmatrix} \boldsymbol{C}^q & -\boldsymbol{c}^e \\ -\boldsymbol{c}^{eT} & \boldsymbol{c}^z \end{bmatrix}, \quad \boldsymbol{C}^q = \boldsymbol{B}^T\boldsymbol{R}^{-1}\boldsymbol{B}, \quad \boldsymbol{c}^e = \boldsymbol{B}^T\boldsymbol{R}^{-1}\boldsymbol{B}^z, \quad \boldsymbol{c}^z = \boldsymbol{B}^z\boldsymbol{R}^{-1}\boldsymbol{B}^z,$$

a symmetrical matrix equation, where $\boldsymbol{C}^m$ is mechanical damping, while $\boldsymbol{C}^e$ is an energy collect matrix.

## 2.5 Energy Flow Equation

Pre-Multiplying Eq. (2-21) by $[\dot{\boldsymbol{q}}^T \quad \dot{\boldsymbol{Z}}^T]$ gives the energy flow equation of system [12],

$$\dot{T} + \dot{D} + \dot{\Pi} = P, \quad T = \frac{1}{2}[\dot{\boldsymbol{q}}^T \quad \dot{\boldsymbol{Z}}^T]\begin{bmatrix} \boldsymbol{M} + \boldsymbol{m}^c & \boldsymbol{0} \\ \boldsymbol{0} & \boldsymbol{m} \end{bmatrix}\begin{bmatrix} \dot{\boldsymbol{q}} \\ \dot{\boldsymbol{Z}} \end{bmatrix}, \quad \dot{D} = [\dot{\boldsymbol{q}}^T \quad \dot{\boldsymbol{Z}}^T]\{\boldsymbol{C}^m + \boldsymbol{C}^e\}\begin{bmatrix} \dot{\boldsymbol{q}} \\ \dot{\boldsymbol{Z}} \end{bmatrix}, \quad (2\text{-}22)$$

$$\Pi = \frac{1}{2}[\boldsymbol{q}^T \quad \boldsymbol{Z}^T]\begin{bmatrix} \boldsymbol{\Lambda} + \boldsymbol{K} & -\boldsymbol{K}^z \\ -\boldsymbol{K}^{zT} & \boldsymbol{k} \end{bmatrix}\begin{bmatrix} \boldsymbol{q} \\ \boldsymbol{Z} \end{bmatrix}, \quad P = [\dot{\boldsymbol{q}}^T \quad \dot{\boldsymbol{Z}}^T]\begin{bmatrix} \boldsymbol{F} \\ \boldsymbol{f} \end{bmatrix}, \quad \hat{P} = [\dot{\boldsymbol{q}}^T \quad \dot{\boldsymbol{Z}}^T]\{\boldsymbol{C}^e\}\begin{bmatrix} \dot{\boldsymbol{q}} \\ \dot{\boldsymbol{Z}} \end{bmatrix}.$$

Here, $T$, $D$ and $\Pi$ are kinetic, dissipated / collected, and potential energies, $P$ total input power by excitations, and $\hat{P}$ collected power. Mechanical designs use damping matrix $\boldsymbol{C}^m$ to reduce vibrations by dissipating vibration energy. In this proposed research, we replace the mechanical damping $\boldsymbol{C}^m$ by electro-magnetic energy harvesting converters with matrix $\boldsymbol{C}^e$ to collect this part of energy and reduce vibrations. For period $\hat{T}$ of track excitation in [13,14], time averaged energy flow equation is

$$\langle\dot{T}\rangle + \langle\dot{D}\rangle + \langle\dot{\Pi}\rangle = \langle P\rangle, \ \langle A(t)\rangle = \frac{1}{\hat{T}}\int_0^{\hat{T}} A(t)\mathrm{d}t. \quad (2\text{-}23)$$

# 3. Solution Approaches

## 3.1 Generalised Integrated Mechanical-Electric Coupling System

Equation (2-17) is an integrated coupling equation, of which the solution reveals its coupling mechanism. The oscillation frequency of LC circuit is in order $1/\sqrt{L\hat{C}}$, much higher than frequencies of vehicle, so that it is neglected.

## 3.2 Approximate Vehicle – Energy Harvester Coupling System

### *3.2.1 Numerical integrations*

In general, time histories of loads are various forms [13,14]. In finite element codes, mode summation and direct integrations are used to solve this equation. Since the damping matrix in Eq. (2-17) is not satisfied normalised conditions, numerical integrations are chosen, such as available program [15].

### *3.2.2 Analytical solution*

For a harmonic excitation of frequency $\Omega$, Eq. (2-21) can be written

$$\begin{bmatrix} \boldsymbol{M}+\boldsymbol{m}^c & \boldsymbol{0} \\ \boldsymbol{0} & \boldsymbol{m} \end{bmatrix}\begin{bmatrix} \ddot{\boldsymbol{q}} \\ \ddot{\boldsymbol{Z}} \end{bmatrix} + \{\boldsymbol{C}^m+\boldsymbol{C}^e\}\begin{bmatrix} \dot{\boldsymbol{q}} \\ \dot{\boldsymbol{Z}} \end{bmatrix} + \begin{bmatrix} \boldsymbol{\Lambda}+\boldsymbol{K} & -\boldsymbol{K}^z \\ -\boldsymbol{K}^{zT} & \boldsymbol{k} \end{bmatrix}\begin{bmatrix} \boldsymbol{q} \\ \boldsymbol{Z} \end{bmatrix} = \widetilde{\boldsymbol{F}}e^{-\mathrm{i}\Omega t}, \tag{3-1}$$

where $\widetilde{\boldsymbol{F}}$ denotes a complex amplitude. The physical force is the real part of complex force,

$$\mathrm{Re}\{\widetilde{\boldsymbol{F}}e^{-\mathrm{i}\Omega t}\} = \mathrm{Re}\{\widehat{\boldsymbol{F}}e^{-\mathrm{i}\vartheta}e^{-\mathrm{i}\Omega t}\} = \widehat{\boldsymbol{F}}\cos(\Omega t+\vartheta). \tag{3-2}$$

The complex dynamic response of forced vibration can be expressed as

$$\begin{bmatrix} \boldsymbol{q} \\ \boldsymbol{Z} \end{bmatrix} = \begin{bmatrix} \boldsymbol{q} \\ \boldsymbol{Z} \end{bmatrix}^{\sim} e^{-\mathrm{i}\Omega t}, \tag{3-3}$$

which, when substituted into Eq. (3-1), gives

$$\widetilde{\boldsymbol{K}}\begin{bmatrix} \boldsymbol{q} \\ \boldsymbol{Z} \end{bmatrix}^{\sim} = \widetilde{\boldsymbol{F}}, \qquad \widetilde{\boldsymbol{K}} = \begin{bmatrix} \boldsymbol{\Lambda}+\boldsymbol{K} & -\boldsymbol{K}^z \\ -\boldsymbol{K}^{zT} & \boldsymbol{k} \end{bmatrix} - \Omega^2\begin{bmatrix} \boldsymbol{M}+\boldsymbol{m}^c & \boldsymbol{0} \\ \boldsymbol{0} & \boldsymbol{m} \end{bmatrix} - \mathrm{i}\Omega\{\boldsymbol{C}^m+\boldsymbol{C}^e\}. \tag{3-4}$$

Here, $\widetilde{\boldsymbol{K}}$ is a complex stiffness matrix. The complex vector of response and its real one are obtained

$$\begin{bmatrix} \boldsymbol{q} \\ \boldsymbol{Z} \end{bmatrix}^{\sim} = \widetilde{\boldsymbol{K}}^{-1}\widetilde{\boldsymbol{F}}, \qquad \begin{bmatrix} \boldsymbol{q} \\ \boldsymbol{Z} \end{bmatrix}^{\wedge} = \mathrm{Re}\left\{\begin{bmatrix} \boldsymbol{q} \\ \boldsymbol{Z} \end{bmatrix}^{\sim} e^{-\mathrm{i}\Omega t}\right\}, \qquad \begin{bmatrix} \dot{\boldsymbol{q}} \\ \dot{\boldsymbol{Z}} \end{bmatrix}^{\wedge} = \mathrm{Re}\left\{-\mathrm{i}\Omega\begin{bmatrix} \boldsymbol{q} \\ \boldsymbol{Z} \end{bmatrix}^{\sim} e^{-\mathrm{i}\Omega t}\right\}. \tag{3-5}$$

The instant input power and harvesting power can be calculated by Eq. (2-22),

$$P = [\dot{\boldsymbol{q}}^T \quad \dot{\boldsymbol{Z}}^T]^{\wedge}\mathrm{Re}\{\widetilde{\boldsymbol{F}}e^{-\mathrm{i}\Omega t}\}, \quad \hat{P} = [\dot{\boldsymbol{q}}^T \quad \dot{\boldsymbol{Z}}^T]^{\wedge}\{\boldsymbol{C}^e\}\begin{bmatrix} \dot{\boldsymbol{q}} \\ \dot{\boldsymbol{Z}} \end{bmatrix}^{\wedge}. \tag{3-6}$$

The time averaged power is calculated by the complex variables with their conjugates $()^*$ as [12]

$$\langle P\rangle = \mathrm{Re}\left\{\{\dot{\widetilde{\boldsymbol{q}}}^T\}\{\widetilde{\boldsymbol{F}}\}^*\right\}, \ \langle \hat{P}\rangle = \mathrm{Re}\left\{\{\dot{\widetilde{\boldsymbol{q}}}^T\}\{\boldsymbol{C}^e\}\dot{\widetilde{\boldsymbol{q}}}^*\right\}, \qquad [\dot{\boldsymbol{q}}^T \quad \dot{\boldsymbol{Z}}^T]^{\sim} = \dot{\widetilde{\boldsymbol{q}}}^T. \tag{3-7}$$

# 4. Example

## 4.1 Governing Equations and Mode Functions

Figure 2 shows a half-integrated beam-like vehicle-energy harvester interaction system, subject to aerodynamic force $f(X,t)$, of mass density $\rho$, length $L$, cross section area $S$ and bending stiffness $EJ$. Using mode summation, its deflection $W(X,t)$ is in Eq. (2-10), where the mode functions are

$$\phi_1(X) = 1/2, \qquad \phi_2(X) = \sqrt{3}X/L, \qquad \int_{-L/2}^{L/2}\phi_n(X)\,\phi_m(X)\mathrm{d}X = \frac{L\delta_{nm}}{4}, \tag{4-1}$$

$$\phi_n(X)=\begin{cases}\frac{1}{2}\{\sinh(2\,\mu_n X/L)/\sinh\mu_n+\sin(2\,\mu_n X/L)/\sin\mu_n\}, n=4,6,\cdots\\ \frac{1}{2}\{\cosh(2\,\mu_n X/L)/\cosh\mu_n+\cos(2\,\mu_n X/L)/\cos\mu_n\}, n=3,5,\cdots\end{cases}, \tag{4-2}$$

The parameter $\mu_1=0=\mu_2$ and the rest $\mu_n$ are positive real roots, given in Table 1, of equation

$$\tan\mu_n+\tanh\mu_n,\quad n=3,5,\cdots;\qquad \tan\mu_n-\tanh\mu_n,\qquad n=4,6,\cdots, \tag{4-3}$$

from which, frequencies $\omega_n$ of beam are calculated by $\omega_n^2=EJ\alpha_n^4/(ML^3)$, $M=\rho SL$. Now, for this example, the matrices and vectors in Eq. (2-17) can be obtained for simulations.

Table 1: The parameter $\alpha_n=\mu_n L$ of free-free beam

| $n$ | 1 | 2 | 3 | 4 | 5 | 6 | 7 |
|---|---|---|---|---|---|---|---|
| $\alpha_n$ | 0 | 0 | 4.7300 | 7.8532 | 10.9956 | 14.1371 | 17.2787 |

Table 2: Fundamental frequencies of track excitations with different track lengths ($V$=300km / h).

| $\lambda$ (m) | 25 | 50 | 100 | 500 | 1000 |
|---|---|---|---|---|---|
| $f_0$ (Hz) | 3.33 | 1.67 | 0.83 | 0.167 | 0.083 |
| $\Omega_0=2\pi f_0$ ($s^{-1}$) | 20.94 | 10.47 | 5.24 | 1.05 | 0.52 |

## 4.2 External Loads

### *4.2.1 Case I: Track excitation*

Based on [13], a road surface excitation is formulated by

$$h_1=h(x,t),\ \ h_2=h(x-2a,t).\quad \dot{h}\ =\begin{cases}\frac{\partial h}{\partial t}+(At+V_0)\frac{\partial h}{\partial x}, & x=\frac{1}{2}At^2+V_0t,\quad A\neq 0,\\ \frac{\partial h}{\partial t}+V\frac{\partial h}{\partial x}, & x=Vt,\quad \text{Constant Speed},\end{cases}, \tag{4-4}$$

where positive or negative value implies convex or concave on track, $A$ and $V_0$ are acceleration and initial velocity of train. An uneven track surface at joint of two tracks of length $\lambda$ is modlled by a periodical excitation

$$h=-\cos\frac{2\pi x}{\lambda},\quad x=Vt,\qquad \dot{h}=\frac{2\pi}{\lambda}V\sin\frac{2\pi x}{\lambda}, \tag{4-5}$$

$$h_1=-\cos\frac{2\pi}{\lambda}Vt,\quad \dot{h}_1=\frac{2\pi}{\lambda}V\sin\frac{2\pi}{\lambda}Vt,\quad h_2=-\cos\frac{2\pi}{\lambda}(Vt-2a),\quad \dot{h}_2=\frac{2\pi}{\lambda}V\sin\frac{2\pi}{\lambda}(Vt-2a).$$

Table 2 shows the fundamental frequencies of track excitations of different track lengths.

### *4.2.2 Case II: Aerodynamic force function*

Paper [14] reported train aerodynamics of different environments, and aerodynamical force distribtution descreasing from vehicle head to tail. The distribuition of pressure on beam in Fig. 3 (a) is adopted. Reference [16] presented an aerodynamic pressure curve by field test [17] in Fig. 3 (b), which shows that the pressure period about 8s, frequnecy 0.125Hz, and its amplitude about 1kPa = $1000\text{Nm}^{-2}$. Based on this result, we assume an aerodynamic force in the form

$$f(X,t)=\beta\hat{f}(X)T(t),\qquad T(t)=\cos\Omega_2 t,\qquad \beta=1000\text{Nm}^{-2},\quad \Omega_2=\pi/4, \tag{4-6}$$

## 4.3 Retained Modes and Results

Considering the track length 1000m with a fundamental frequency 0.083Hz in Table 2, and the frequency of aerodynamic force is 0.125Hz, much less that the first elastic frequency of beam 8.43Hz [18], we retain two rigid beam modes for numerical analysis, and have

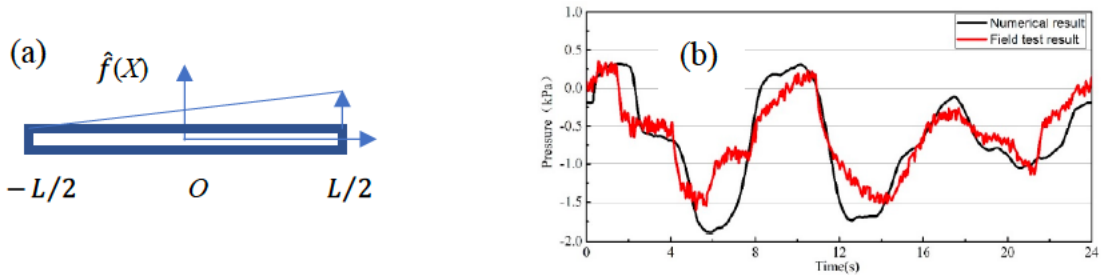


Figure 3: (a) Spacial distribution $\hat{f}(X) = X/L + 1/2$ of aerodynamic pressure on the beam in equation (4-1); (b) Aerodynamic pressure at a tunnel entry obtained by simulation [16] and field test [17].

$$\boldsymbol{\Phi} = [\phi_1 \quad \phi_2], \quad \boldsymbol{q} = [q_1 \quad q_2]^{\mathrm{T}}, \quad \boldsymbol{F} = \beta \begin{bmatrix} F_1 \\ F_2 \end{bmatrix} \cos \Omega_2 t, \; F_1 = \frac{L}{4}, \quad F_2 = \frac{\sqrt{3}L}{12}, \tag{4-7}$$

$$\phi_1 = 1/2, \quad \phi_2 = \sqrt{3}X/L, \quad \phi_1(X_1) = 1/2 = \phi_1(X_2), \quad \phi_2(X_1) = \sqrt{3}a/L = -\phi_2(X_2),$$

$$\boldsymbol{M} = \frac{M}{4}\mathbf{I}, \quad \boldsymbol{m} = m^{\mathrm{b}}\mathbf{I}, \quad \boldsymbol{\Lambda} = \mathbf{0}, \quad \boldsymbol{K} = K\begin{bmatrix} 1/2 & 0 \\ 0 & 6a^2/L^2 \end{bmatrix}, \quad \boldsymbol{K}^z = K\begin{bmatrix} 1/2 & 1/2 \\ \sqrt{3}a/L & -\sqrt{3}a/L \end{bmatrix}, \quad \boldsymbol{k} = (K+k)\mathbf{I},$$

$$\boldsymbol{C}^m = \begin{bmatrix} \mathbf{0} & \mathbf{0} \\ \mathbf{0} & c\mathbf{I} \end{bmatrix}, \quad \boldsymbol{C}^e = C^e \begin{bmatrix} \boldsymbol{C}^q & -\boldsymbol{c}^e \\ -\boldsymbol{c}^{eT} & \mathbf{I} \end{bmatrix}, \quad \boldsymbol{C}^q = \begin{bmatrix} 1/2 & 0 \\ 0 & 6a^2/L^2 \end{bmatrix}, \quad \boldsymbol{c}^e = \begin{bmatrix} 1/2 & 1/2 \\ \sqrt{3}a/L & -\sqrt{3}a/L \end{bmatrix}, \quad C^e = \frac{B^2 l^2}{R+r},$$

$$M = 19000\mathrm{kg}, \quad m^{\mathrm{b}} = 2500\ \mathrm{kg}, \quad K = 1.016 \times 10^6 \mathrm{Nm}^{-1}, \quad k = 4.935 \times 10^6,$$

$$V = 250/3\ \mathrm{m\,s}^{-1}, \quad c = 5.074 \times 10^4\ \mathrm{Nsm}^{-1}, \quad L = 22\mathrm{m}, \quad a = 9.3\mathrm{m}, \quad \lambda = 1000\mathrm{m}.$$

Here, $C^e$ is a paramter controled to check the perfomance of system. Figs. 4 and 5 give the results for Cases I and II, which shows that with $C^e$ increasing, harvested power increases and vibrations reduced.

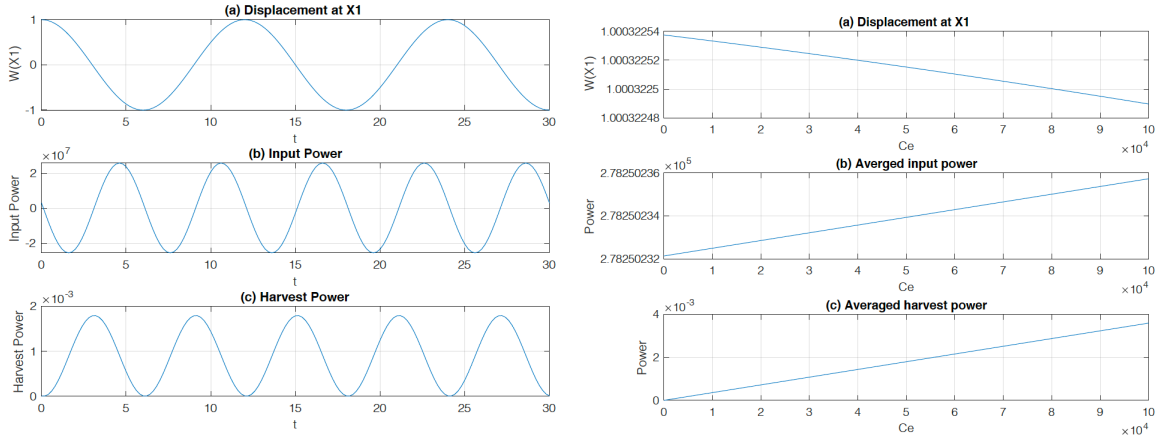


Figure 4: Case I track excitation: left time histories ($C^e = 50000$); right amplitudes for the displacement at point $X_1$, input power and harvested power.

## 5. Conclusion and Discussions

A mathematical model governing a railway vehicle-electromagnetic energy harvester coupling system is developed and investigated, providing a means to design suspension units in high-speed trains to reduce vibrations and harvest energies. The example shows that with increasing energy harvesting parameter, vibrations are reduced while harvested power is increased. The paper is a theoretical and numerical work, based on which real designs involving practical cases need to be further addressed.

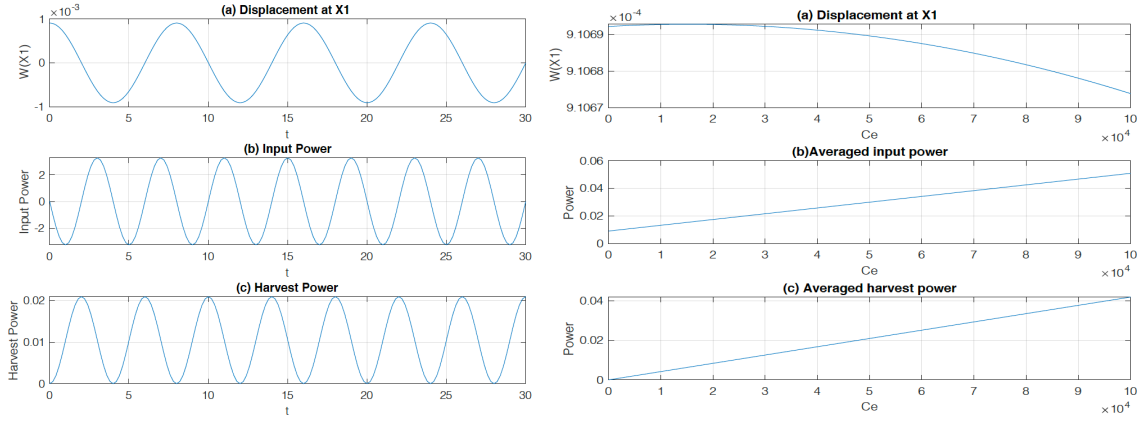


Figure 5: Case II aerodynamic excitation: left time histories $C^e = 50000$; right amplitudes for the displacement at point $X_1$, input power and harvested power.

# REFERENCES


1 Thorpe, T.W. *A brief review of wave energy, a report produced for The UK Department of Trade and Industry*, ETSU R-120, AEA Technology Plc. (1999)

2 Office of Naval Research. *Environmental Assessment for Proposed Wave Energy Technology Project in Kaneohe Bay, Hawaii.* Report by Office of Naval Research and US Department of the Navy, (2003)

3 Paasch, R., Ruehl, K., Howland, J., Meicke, S. Wave energy: a Pacific perspective. *Phil. Tran. R. Soc.* A 370 (2012) 481-501

4 Xing, J.T. Developments of numerical methods for linear and nonlinear fluid-solid interaction dynamics with applications. *Adv. Mech.*, 46 (2006) 201602

5 Karnopp, D. Permanent magnet linear motors used as variable mechanical dampers for vehicle suspensions. *V. Sys. Dyn.* 18 (1989) 187–200

6 Karnopp, D. Power requirement for vehicle suspension systems. *V. Sys. Dyn.* 21 (1992) 65–71.

7 Zhang, Y., Yu, F., Huang, K. A state of art review on regenerative vehicle active suspension, *Proc. 3rd Int. Conf. Mech. Eng. Mech.* (ICMEM), Beijing, China, 2009

8 Zuo, L., Tang, X. Large-scale vibration energy harvesting. *J. Intel Mat Sys & Structures* 24 (2013) 1405-1430

9 Foo, E., Goodall, R.M. Active suspension control of flexible-bodied railway vehicles using electro-hydraulic and electro-magnetic actuators. *Con. Eng. Practice* 8, (2000) 507-518

10 Wei, W., Li, Q,. Xu, F., Zhang, X., Jin, J., Sun, F. Research on an electromagnetic actuator for vibration suppression and energy regeneration. *Actuators* 9 (42), (2020) 1-17

11 Xing, J.T., Sun, Z., Zhou, S., Tan, M. Dynamic interactions of an integrated vehicle-electromagnetic energy harvester-tire system subject to uneven road excitations. *Acta Mech. Sin.* 33(2), (2017) 440-456.

12 Xing, J.T. *Energy Flow Theory of Nonlinear Dynamical Systems with Applications*, Springer, Heidelberg (2015)

13 Zhang, S., Fan, W. Steady-state dynamic analysis of the vehicle-pavement interaction system subjected to road surface excitation. *8th Int. Conf. Vib. Eng.*, Paper ID: S07-07, 24-26 July 2021, Shanghai, China (2021)

14 Tian, H.Q. Review of research on high-speed railway aerodynamics in China. *Trans. Safety and En.*, 1(1), (2019) 1–21.

15 Xing, J.T. *Fluid-solid interaction dynamics: theory, variational principles, numerical methods, and applications.* Elsevier, London, (2019) and HEP Beijing (2021)

16 Hu, Y., Ge, X., Wang, C., Zhang, H., Ling, L., Wang, K. Dynamic performance of high-speed train passing through a tunnel exit under crosswind. *8th int. conf. vib. eng.*, ID: S07-06, 24-26 July 2021, Shanghai, China

17 Han, K., Tian, H.Q. Research and application of testing technology of aerodynamics at train tunnel entry on special passenger railway lines. *J. Cen. South Univ. (Sc & Tech),* 82(2), (2007), 326-332

18 Foo, E., Goodall, R.M. Active suspension control of flexible-bodied railway vehicles using electro-hydraulic and electro-magnetic actuators. *Con. Eng. Prac.* 8, (2000) 507-518